analytical chemistry

Article

pubs.acs.org/ac

On-Tissue Derivatization via Electrospray Deposition for Matrix-Assisted Laser Desorption/Ionization Mass Spectrometry Imaging of Endogenous Fatty Acids in Rat Brain Tissues

Qian Wu, Troy J. Comi, Bin Li, Stanislav S. Rubakhin, and Jonathan V. Sweedler*

Department of Chemistry and the Beckman Institute, University of Illinois at Urbana−Champaign, Urbana, Illinois 61801, United States

Supporting Information

ABSTRACT: Matrix-assisted laser desorption/ionization (MALDI) mass spectrometry imaging (MSI) is used for the multiplex detection and characterization of diverse analytes over a wide mass range directly from tissues. However, analyte coverage with MALDI MSI is typically limited to the more abundant compounds, which have m/z values that are distinct from MALDI matrix-related ions. On-tissue analyte derivatization addresses these issues by selectively tagging functional groups specific to a class of analytes, while simultaneously changing their molecular masses and improving their desorption and ionization efficiency. We evaluated electrospray deposition of liquid-phase derivatization agents as a means of on-tissue analyte derivatization using 2-picolylamine; we were able to detect a range of endogenous fatty acids with MALDI MSI. When compared with airbrush application, electrospray led to a 3-fold improvement in detection limits and decreased analyte delocalization. Six fatty acids were detected and visualized from rat cerebrum tissue using a MALDI MSI instrument operating in positive mode. MALDI MSI of the hippocampal area allowed targeted fatty acid analysis of the dentate gyrus granule cell layer and the CA1 pyramidal layer with a 20-μm pixel width, without degrading the localization of other lipids during liquid-phase analyte derivatization.

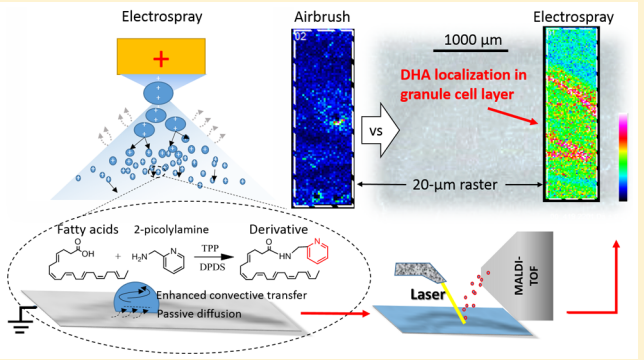

Mass spectrometry imaging (MSI)[1] is a sensitive, multiplex, and nontargeted approach for the detection and characterization of a wide range of analytes in a variety of biological and clinical samples. MSI uses several ionization techniques, including secondary ion mass spectrometry (SIMS), laser desorption/ionization (LDI), desorption electrospray ionization (DESI), and matrix-assisted laser desorption/ionization (MALDI).[2] Of these, MALDI provides the widest mass range[3−6] while obtaining micrometer-scale spatial resolution and detection limits comparable to other MSI approaches.[7,8] MALDI MSI is well suited for the simultaneous localization of small metabolites,[3,4] lipids,[9] and peptides[10] in tissues. The resultant multiplex chemical images help to reveal molecular mechanisms of disease,[11] facilitate biomarker discovery,[12] and enable tracking of specific molecular classes such as cell−cell signaling molecules.[13]

Although MALDI MSI has many advantages, the method does have some shortcomings. It is limited by sensitivity (impacting lower concentration analytes) and is subject to matrix interference in the low m/z range,[14] delocalization of analytes during matrix deposition, and ion suppression from more abundant molecules.[15] An example of the potential limitation of MALDI MSI has been in the investigation of fatty acids, critical components of lipid metabolism that are incorporated in triacylglycerides of fat droplets stored in the cytosol of adipocytes. Free fatty acids (FFAs)[16] are involved in the synthesis of different structural and signaling molecules that are critical for various cellular processes such as lipid and glucose metabolism. However, because of their low molecular weight (200−400 Da), low abundance in tissue, and poor ionization efficiency, direct MALDI MSI of these molecules in tissues using traditional matrixes such as 2,5-dihydroxy benzoic acid (DHB) or 9-aminoacridine (9-AA) has been challenging. A variety of low-background MALDI MS matrixes, e.g., silicon nanoparticles,[17] graphite,[18] pencil lead,[19] powdered carbon aerogels,[20] silver/gold nanoparticles,[21,22] and graphene,[23] have been introduced and applied to fatty acid detection, resulting in high coverage and sensitivity for FFAs.[18,20,23] However, these techniques may restrict detection of other classes of analytes compared to traditional matrixes,[24] frequently due to their affinity for specific classes of molecules[21,22,25] or fragmentation of higher molecular weight analytes.[26,27] Moreover, few of these approaches have been applied to the characterization of FFAs by MSI.[21,22] Time-of-flight (TOF)-SIMS is commonly utilized for FFA imaging in tissue sections but typically fragments large molecular ions.[28,29] For MALDI-based imaging, high-mass

Received: March 14, 2016
Accepted: May 14, 2016
Published: May 14, 2016

DOI: 10.1021/acs.analchem.6b01021
Anal. Chem. 2016, 88, 5988−5995

resolution instruments such as Fourier transform ion cyclotron resonance (FTICR)[30,31] can discriminate FFAs from MALDI matrix interference in brain tissue sections. Because of the high cost and low sampling rate, FTICR may not be suitable for some analyses; therefore, an efficient MALDI-TOF MSI method that is sensitive to FFAs using a traditional MALDI matrix would be a valued alternative.

On-tissue or in-tissue chemical derivatization methods have been developed for MALDI MSI to improve sensitivity for specific classes of biomolecules. These techniques utilize a molecular tag that reacts with analytes of interest to increase the molecular mass of small molecules and enhance their ionization efficiency.[32−36] In highly selective reactions, other endogenous compounds are left unchanged, enabling MALDI MS using a traditional matrix and producing mass spectra comparable with the underivatized data available in MS databases. In prior studies,[32,33,35−37] derivatization reagents have been deposited onto tissue via spray or sublimation. Several other protocols have been described. In one, tissues are placed in a chamber containing solvent vapor to develop the chemical reaction for 10−60 min; the derivatization provides high yields but the extended derivatization time may lead to analyte delocalization.[15] Another option utilizes an automated microspotting device to deposit the derivatization reagent in picoliter-volume droplets onto the tissue.[34] The spatial resolution of MSI in this case is limited by the distance between individual spots as well as solution deposition and incubation times. As a final example, a derivatization reagent was applied on the sample plate before tissue thaw-mounting, without extended reaction in a chamber, and produced images at 50-μm spatial resolution.[38] Oftentimes analyte derivatization reactions proceed too slowly or have specific requirements for solution composition, making them less suitable for derivatization reagent precoating. Many MSI methods that use derivatization have produced spatial resolutions poorer than 100 μm.

Here we describe an alternative derivatization approach based on electrospray deposition. Electrospray[39−41] forms a plume of microdroplets, emitted from a solution placed in contact with one electrode and directed toward a second electrode, with high potential differences between the two. The resulting droplets often have diameters in the nanometer range.[40] Electrospray is widely used as a soft ionization method but also is suitable as a solvent and solute deposition method. Earlier studies utilized electrospray for MALDI matrix deposition in MSI applications,[31,42,43] but due to rapid drying of the small droplets, this deposition method substantially limited analyte incorporation into the matrix.[31] Guo et al.[30] recently described a related technique where an electric field was applied while depositing matrix by piezoelectric nebulization, enhancing the detection of small molecules.

Using electrospray deposition, we applied reagents for *in situ* derivatization and extraction of fatty acids from well-defined tissue areas in the rat brain. We expected that implementing the electrospray without a sheath gas would generate highly charged, nanoscale derivatization reagent droplets with enhanced extraction and derivatization efficiencies for fatty acids while maintaining native FFA distributions. We used 2-picolylamine (PA) to derivatize fatty acids by forming an amide bond with the carboxyl group of FFAs in the presence of 2,2-dipyridyl disulfide (DPDS) and triphenylphosphine (TPP). The reaction occurs quickly over a broad temperature range (20−60 °C), making it suitable for *in situ* derivatization.[44,45] Our results not only demonstrate the effectiveness of electrospray deposition of derivatization agents onto biological specimens, the approach achieved improved sensitivity compared to traditional airbrush application and a spatial resolution of 20 μm for the multiplex analysis of FFAs with MALDI MSI.

EXPERIMENTAL SECTION

Chemicals. Docosahexaenoic acid (DHA, purity ≥98%), linolenic acid (purity ≥99%), linoleic acid (purity ≥99%), and palmitoleic acid (purity ≥98.5%) were purchased from Sigma-Aldrich (St. Louis, MO). Stock solutions (1 mg/mL) of the standards were prepared in acetonitrile (ACN) and stored at −20 °C. The ACN, water, acetic acid (all liquid chromatography (LC)/MS grade), and ammonium acetate (purity ≥97%) were from Fisher Scientific (Pittsburgh, PA). The TOF mass analyzer was calibrated with the Bruker Daltonics Inc. (Billerica, MA) Peptide Calibration Standard II (containing bradykinin, angiotensin II, angiotensin I, substance P, bombesin, ACTH clip 1-17, ACTH clip 18-39, renin substrate, and somatostatin 28). The derivatization reagent PA (purity ≥99%) and activation reagent TPP (purity ≥99%) were purchased from Sigma-Aldrich, and the activation reagent DPDS (purity ≥98%) was acquired from Tokyo Chemical Industry (Tokyo, Japan); 9-AA (purity ≥98%) and DHB (purity ≥98%) were from Sigma-Aldrich (St. Louis, MO).

Tissue Preparation and Sectioning. Tissues were harvested from four male Sprague−Dawley rats (Harlan Laboratories, Indianapolis, IN), 1−3 months old, maintained on a 12-h light/dark cycle and fed normal chow *ad libitum*. Euthanasia by decapitation was performed in compliance with local and federal regulations and according to animal use protocols approved by the Illinois Institutional Animal Care and Use Committee.

In all cases, the brains were surgically dissected, frozen in liquid nitrogen, and stored at −80 °C until use. Coronal tissue sections, 18-μm thick, were prepared from frozen cerebrum using a cryostat (3050S, Leica Biosystems Inc., Buffalo Grove, IL) at −19 °C and thaw-mounted onto conductive indium−tin oxide (ITO)-coated glass slides (Delta Technologies, Loveland, CO).

Details on the preparation and usage of the four animals are described in the in the Supporting Information. While most samples were analyzed immediately following preparation, some sections were stored at −80 °C for later use. Optical images of the tissues were taken using a flatbed scanner (Epson Perfection V300, Epson America, Inc., Long Beach, CA) with a resolution of 2400 dpi before MSI. The optical images shown in Figure 3 were adjusted to aid in visualization of hippocampal structures using Adobe Photoshop 2014.

Sample Preparation for MALDI MSI. Samples were thawed and dried in an N_2-filled desiccator for 20 min. For the optimization experiments, 2 μL of DHA standard solutions with gradient concentrations ranging from 0.15 to 12.5 ng/mm^2 were deposited on one slide and then dried in an N_2-filled desiccator for 20 min. The derivatization solution, comprised of 2 mM of the derivatization reagent (PA) with 10 mM of the activation reagents (TPP and DPDS) in ACN, was applied on the specimen by electrospray or airbrush. Electrospray was performed with a laboratory-constructed system (Figure S1A). The derivatization solution was delivered through a fused-silica capillary (250-μm inner diameter (i.d.), 365-μm outer diameter) electrospray emitter via a syringe pump (Harvard

DOI: 10.1021/acs.analchem.6b01021
Anal. Chem. 2016, 88, 5988−5995

Apparatus, Inc., Holliston, MA) at variable flow rates (0.5−4 mL/h), with deposition times lasting between 1−5 min. An optimized high voltage (6000 V) was applied to the spray nozzle with the tissue-coated slide held at ground to generate a stable Taylor cone at an emitter-to-tissue distance of approximately 3 cm. For airbrush deposition, conditions were selected based on previous tissue derivatization studies, with minor modifications.[32,35,36] Briefly, 1 mL of the derivatization solution was applied with a 0.2 mm nozzle caliber airbrush (Paasche Airbrush Company, Chicago, IL), with a nozzle-to-target distance of 50 cm and nozzle nitrogen gas pressure of 20 psi.

Following derivatization, target plates were coated with MALDI matrix (either 9-AA or DHB) using a laboratory-constructed sublimation system (Figure S1B), similar to previously published work,[46] with some modifications.[47] The detailed procedure is described in the Supporting Information. The final matrix thickness was ∼500 $\mu g/cm^2$, determined by comparing tissue weight before and after sublimation.

For comparison to the underivatized samples, the matrix was deposited by sublimation using identical conditions, except that the DHB sublimation required a coating time of 11.5 min and 9-AA required 15 min.

Sample Preparation for LC−Tandem MS (MS/MS). Unused tissue that remained after sectioning for MALDI MSI was punched with a tissue punch (1 mm i.d.) while the tissue remained frozen in the cryostat. Punches were taken at specific regions: the isocortex, hippocampal formation, thalamus, fiber tract, olfactory area, and hypothalamus. The length of each tissue punch was determined with a microslide field finder and used in estimating sample volume. Punches were homogenized in 600 μL of ethanol with 10 min of sonication on ice in a bath sonicator (8891 Ultrasonic Cleaner, Cole-Parmer, Vernon Hills, IL). The extracts were centrifuged at 6600g at 4 °C for 5 min, and the supernatants were collected and divided into three equal aliquots for three replicate measurements after the following sample preparation steps: extract solutions were dried with a gentle N_2 stream at ambient conditions; derivatization solution (200 μL) was added to each dried sample and incubated for 10 min at room temperature (RT) (RT = 25 °C throughout) for derivatization. The derivatized extracts (2 μL) were directly injected into the LC system to validate the MALDI MSI results.

MALDI MSI, MALDI MS/MS, and LC−MS/MS Analyses. MALDI-TOF MSI was conducted with an ultrafleXtreme mass spectrometer (Bruker) equipped with a solid-state UV Smartbeam II laser. The laser was set to the "ultra" setting with an ∼100-μm diameter footprint for low-resolution imaging and the "small" setting with an ∼20-μm diameter footprint for high-resolution imaging. The acquisition from each pixel was the sum of 1000 laser shots at 1000 Hz laser frequency, 70% laser intensity, and 120 ns pulsed ion extraction time. MALDI MS spectra were acquired in the m/z range of 20 to 3000. Laser intensity and pulsed ion extraction time were selected to optimize peak intensity while obtaining sufficient mass resolution, here about 5000, in the mass range between 300 to 400 Da. A mixture of DHB, bradykinin, and angiotensin II was deposited near to the brain tissue section to minimize mass error from surface topography. Image acquisition was performed with flexImaging software (version 3.0, Bruker) using raster steps between 20 to 300 μm.

MS/MS analysis was used to confirm the structure of the detected fatty acids. The LIFT mode of the MALDI mass spectrometer was used with argon as a collision gas and a 2 Da precursor isolation window.

LC−MS/MS was performed using an EVOQ Elite triple quadrupole mass spectrometer (Bruker) connected to an Advance UHPLC system (Bruker). The LC separation conditions, MS detection conditions, and subsequent quantitation of the LC−MS/MS data are provided in the Supporting Information.

Processing and Statistical Analysis of MALDI MSI Data. The molecular ion distribution images of tissue sections were visualized using flexImaging. MALDI MSI data acquired from triplicate brain slices from the same rat and thaw-mounted on three separate slides were used in the statistical analysis. Statistical comparisons of peak intensities from different brain regions were performed by exporting data from manually defined regions of interest (ROI) corresponding to the punched regions analyzed with LC−MS/MS. Mass spectra in each ROI were imported into ClinProTools (Bruker) with automatic baseline subtraction and total ion count normalization. Peaks were picked with a signal/noise threshold greater than 3 on average spectra and matrix-related peaks were removed. Picked peaks were exported as m/z value-peak intensity tables. Peak intensities were root-mean-square-normalized prior to calculating mean peak intensities. The mean values were used to calculate the relative standard deviation (RSD) of the triplicate measurements. For comparison of the averaged peak intensities of signals acquired from different brain regions, a two sample t-test was calculated using OriginPro 8.5 (OriginLab Corporation, Northampton, MA) to determine significant differences between the average peak intensities of each pair of regions measured in triplicate. Resulting p-values for each pair were false discovery rate (FDR)-corrected with a Benjamini and Hochberg's FDR-controlling procedure with $c(N) = 1$.

RESULTS AND DISCUSSION

MALDI MSI of Endogenous FFAs in Rat Brain Tissue without Derivatization. The ability to detect the tissue distributions of important signaling molecules, such as FFAs, leads to improved understanding of the mechanisms of

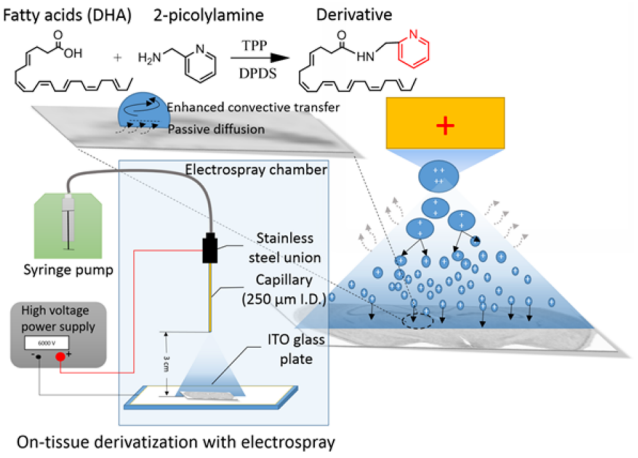

Figure 1. Schematic illustration of on-tissue analyte derivatization via electrospray deposition of reagents. A 250-μm i.d. fused-silica capillary is used as an emitter in the electrospray system and is positioned 3 cm above the tissue slice located on an ITO-glass slide. Inset: the derivatization reaction scheme.

DOI: 10.1021/acs.analchem.6b01021
Anal. Chem. 2016, 88, 5988−5995

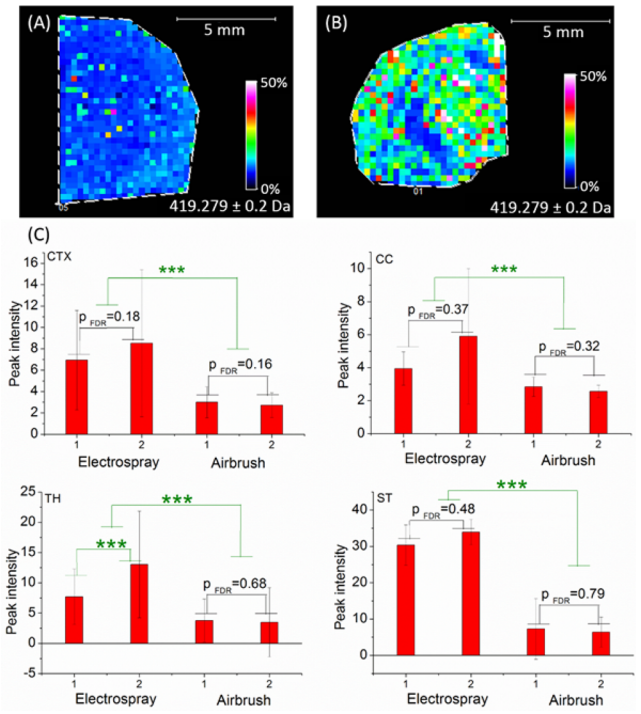

Figure 2. MALDI MSI ion maps (300 μm pixel width) of DHA using on-tissue derivatization with (A) airbrush and (B) electrospray as the deposition methods. (C) The average intensity of DHA, with the standard deviation shown as error bars, from different subregions of the cerebrum: CTX, cortex; CC, corpus callosum; TH, thalamus; and ST, spotted standards. (Experimental duplicates were labeled as electrospray 1 and 2 and airbrush 1 and 2). *P* values were calculated by the two-sample *t*-test between the data pointed by the end of the line. *** indicates *p* value of <0.001.

different cellular processes, including lipid and glucose metabolism. Although FFAs have been imaged using TOF-SIMS[28,29] and MALDI-FTICR-MSI,[30,31] a MALDI-TOF MSI method provides the ability to examine FFA distributions in the context of other biomolecules, and at lower cost. However, using existing protocols, FFA signals are obscured by common matrix peaks, which are abundant in the low mass range. With TOF mass analyzers these signals are difficult to resolve, making MALDI-TOF MSI of FFAs problematic.[18,20,23]

To assess the feasibility of underivatized MSI of FFAs, the MALDI matrixes DHB and 9-AA were applied to rat brain tissue for negative-mode MSI. As shown in Figure S2, the m/z range corresponding to important fatty acids (such as linoleic acid and arachidonic acid (AA)) is heavily obscured by numerous background peaks that interfere with the detection of targeted analytes, particularly with the matrix 9-AA (Figure S2B). Furthermore, the low ionization efficiency of FFAs and subsequent lower sensitivity in negative-mode MALDI-TOF MS was exacerbated in chemically and structurally complex brain tissue. Only m/z values consistent with oleic acid and erucic acid were detectable in negative mode with low intensity in rat brain tissue. For DHB-coated tissues (Figure S2A), no detectable signal was observed for m/z values corresponding to targeted fatty acids such as DHA, linoleic acid, and palmitoleic acid. Several strong background peaks from DHB were detected, overlapping with fatty acid m/z values consistent with eicosapentaenoic, arachidonic, and linolenic acids.

Development of On-Tissue Chemical Derivatization for FFAs with Electrospray Deposition of Reagents. A prior study[45] demonstrated that primary or secondary amino groups can be condensed with a carboxyl group in the presence of different activation agents such as DPDS-TPP (also named Mukaiyama A solution). This reaction proceeds with rapid kinetics when performed in ACN and reaches equilibrium after 10 min at RT.[45] These properties make it appealing as an on-tissue derivatization scheme.

In our initial, solution-phase derivatization experiments, a 2 mM PA derivatization reagent with 10 mM DPDS and 10 mM TPP reacted with five fatty acid standards at RT with equivalent peak intensities as were observed at 60 °C. The derivatized fatty acids were detected with a 91 Da mass shift, consistent with the condensation observed using PA.

A requirement of on-tissue derivatization is rapid mixing of the reagents with analytes dispersed throughout the tissue. With spray-based reagent application, heterogeneous-phase mass transfer is involved and the reaction is controlled by the diffusion of analyte and reagent in the solution layer adjacent to the tissue.[48,49] Moreover, the reaction time affects the overall reaction efficiency. Thus, many parameters controlling the reagent diffusion rate and reaction time, such as droplet size, reagent concentration, and convection in droplets, will affect the reaction yield and kinetics.

In previous studies,[32,33,35−37] derivatization reagents were applied to tissues with nebulizing spray- or sublimation-based approaches, followed by incubation in a reaction chamber saturated with solvent vapor for several hours. For our chosen reaction scheme, sublimation was not feasible due to the liquid state of the derivatization reagent at RT. We also expected that spray application would generate larger, nonuniform droplets on tissue, leading to FFA delocalization. Analyte delocalization worsens with the longer incubation time required to fully develop spray-based derivatization. To reduce these adverse effects, we used electrospray to apply the derivatization and activation reagents (Figure 1). The electrospray process generates smaller droplets[39−41] than those produced by nebulization with an airbrush, limiting delocalization of analytes following tissue impact. Additionally, the charged droplets may impact with higher velocities due to the electric field,[50,51] causing higher shear stress on impact,[52,53] and perhaps facilitating mixing with the FAs in the tissue. Electrospray deposition appears to reduce the required reaction time.

To determine the optimal electrospray conditions for derivatization, we spotted DHA standard solution on ITO-glass slides and applied our derivatization reagent employing different electrospray parameters by varying infusion flow rate, deposition time, and derivatization reagent concentration (Figure S3). Increasing the infusion flow rate significantly increased the observed peak intensity. Furthermore, increasing the deposition time from 1 to 3 min led to significant improvements in peak intensity, whereas a longer deposition time of 5 min showed no additional improvement.

However, other performance metrics are important when applying electrospray deposition to tissue sections for MSI. While higher flow rates improve signal intensity, they may also lead to larger droplets, which cause delocalization of analytes on tissue (Figure S4B,C). A flow rate of 2 mL/h provided a suitable compromise between intensity and resolution and generated ion images with distinguishable dentate gyrus layers of the hippocampus area (Figure S4D). Subsequent on-tissue derivatization was performed at 2 mL/h with 2 mM of the derivatization reagent and 10 mM of the activation agents, with a 3 min deposition time. With the optimized conditions, a limit

DOI: 10.1021/acs.analchem.6b01021
Anal. Chem. 2016, 88, 5988−5995

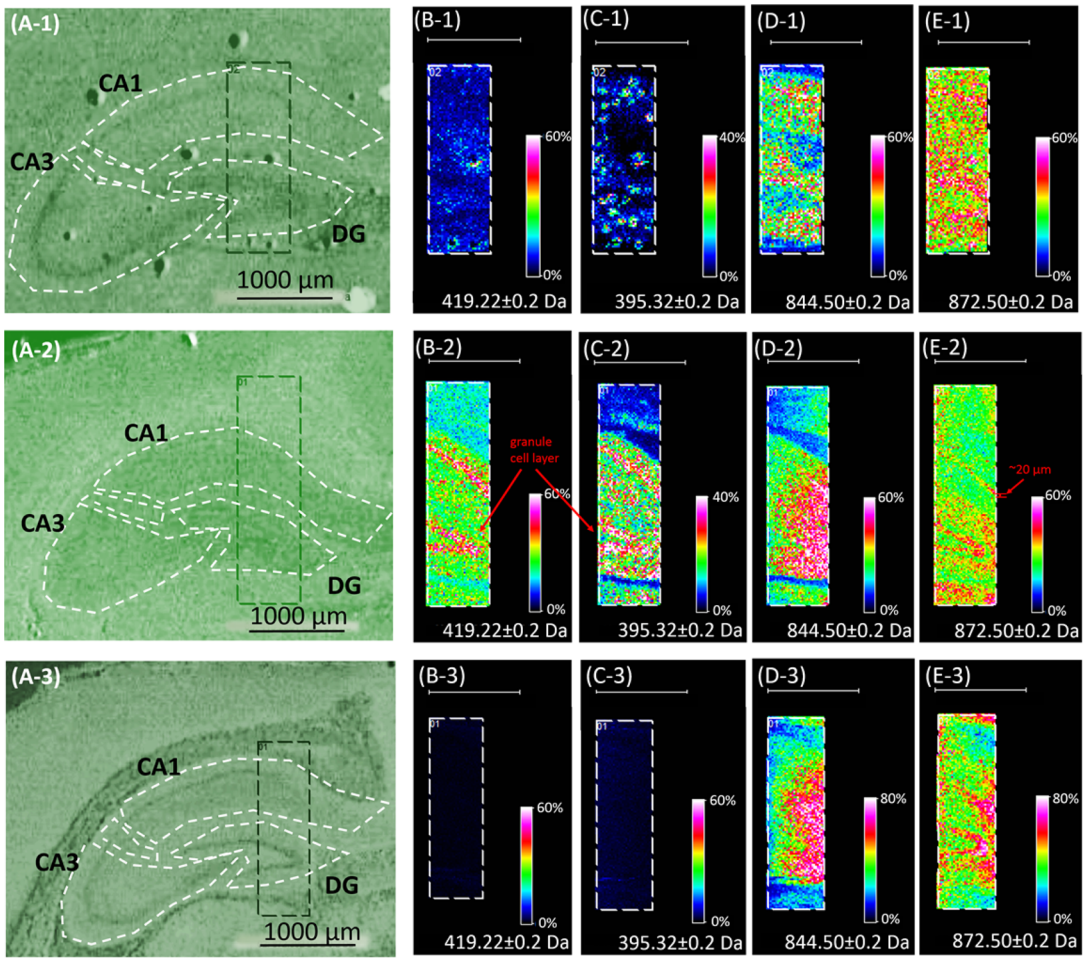

Figure 3. (A) Optical images (subfields were outlined by comparison to prior brain maps[54]) of rat cerebrum tissue sections. Boxed areas in panels A indicate the hippocampal area and correspond to the boxes in Panels B–E. (B–E) High-resolution MALDI MSI ion maps (20 μm pixel width) from the hippocampal area (boxed). (B) DHA, (C) AA, (D) PC (38:6) (m/z 844.6), and (E) PC (40:6) (m/z 872.6); 1 = derivatization with airbrush, 2 = derivatization with electrospray, and 3 = no derivatization, showing the spatial resolution and lipid delocalization before and after derivatization. Scale bars (B–E) = 1000 μm.

of detection for DHA down to about 8 pg/mm^2 can be obtained with good linearity (R^2 = 0.9921) over a range of 150 pg/mm^2 to 6.25 ng/mm^2 (Figure S3D).

Comparison of Electrospray and Airbrush Derivatization Reagent Applications. To compare imaging results between airbrush and electrospray applications, low-resolution images (300 μm) (Figure 2A,B) and high-resolution images (20 μm) (Figure 3B–E) were obtained for each sample set. For low-resolution imaging, standard spots and select subregions of the cerebrum were chosen as ROIs for further statistical analysis. The airbrush-treated samples had significantly lower intensity than the electrospray ($p < 0.05$) for standard spots (n = 3) and for three distinct cerebrum subregions (Figure 2C).

To compare the spatial resolution of each approach, a 20-μm laser and raster size were used. As shown in Figure 3B-1, C-1, several spots of high intensity are present following the airbrush application, perhaps from a nonuniform deposition of large reagent droplets. In contrast, electrospray deposition displays clear localization of DHA, AA, and two phosphatidylcholine (PC) lipids to specific cell layers of the hippocampus (Figure 3B-2–E-2) according to our optical images and known brain anatomical structures.[54] We can localize FFAs to specific layers on the order of 20 μm, the same as our raster spacing. Thus, it appears electrospray deposition does not lead to obvious delocalization of fatty acids during sample preparation.

MALDI-TOF MSI of FFAs in Rat Brain Tissue with On-Tissue Chemical Derivatization. Using the optimized conditions, another rat cerebrum was sectioned for on-tissue derivatization experiments. MALDI MS images (Figure 4B), at low resolution (100 μm) of the entire cerebrum and high resolution (20 μm) for the hippocampus area, were acquired in positive mode, with a representative spectrum shown in Figure 4A. Following on-tissue derivatization, nine fatty acids were detected, including seven unsaturated fatty acids (DHA, AA, oleic acid, linolenic acid, palmitoleic acid, eicosapentaenoic acid, and linoleic acid) and two saturated fatty acids (stearic acid and palmitic acid). The FFAs were putatively identified *in situ* with MALDI-TOF/TOF MS. As shown in Figure 4C, the MS/MS mass spectra of derivatized fatty acid standards display a characteristic fragment at m/z 108, also detected in rat tissue samples, which corresponds to the derivatization reagent [PA ($C_5H_4NCH_2NH_2$)]$^+$ following amide bond cleavage.[44] Most MS/MS spectra of detected fatty acids in tissue have identical fragments with that of DHA standards (Figure S5), except linoleic acid and linolenic acid, which also had several other abundant fragments, presumably from isobaric precursor ions. We performed MS/MS, although the detailed structures of

DOI: 10.1021/acs.analchem.6b01021
Anal. Chem. 2016, 88, 5988–5995

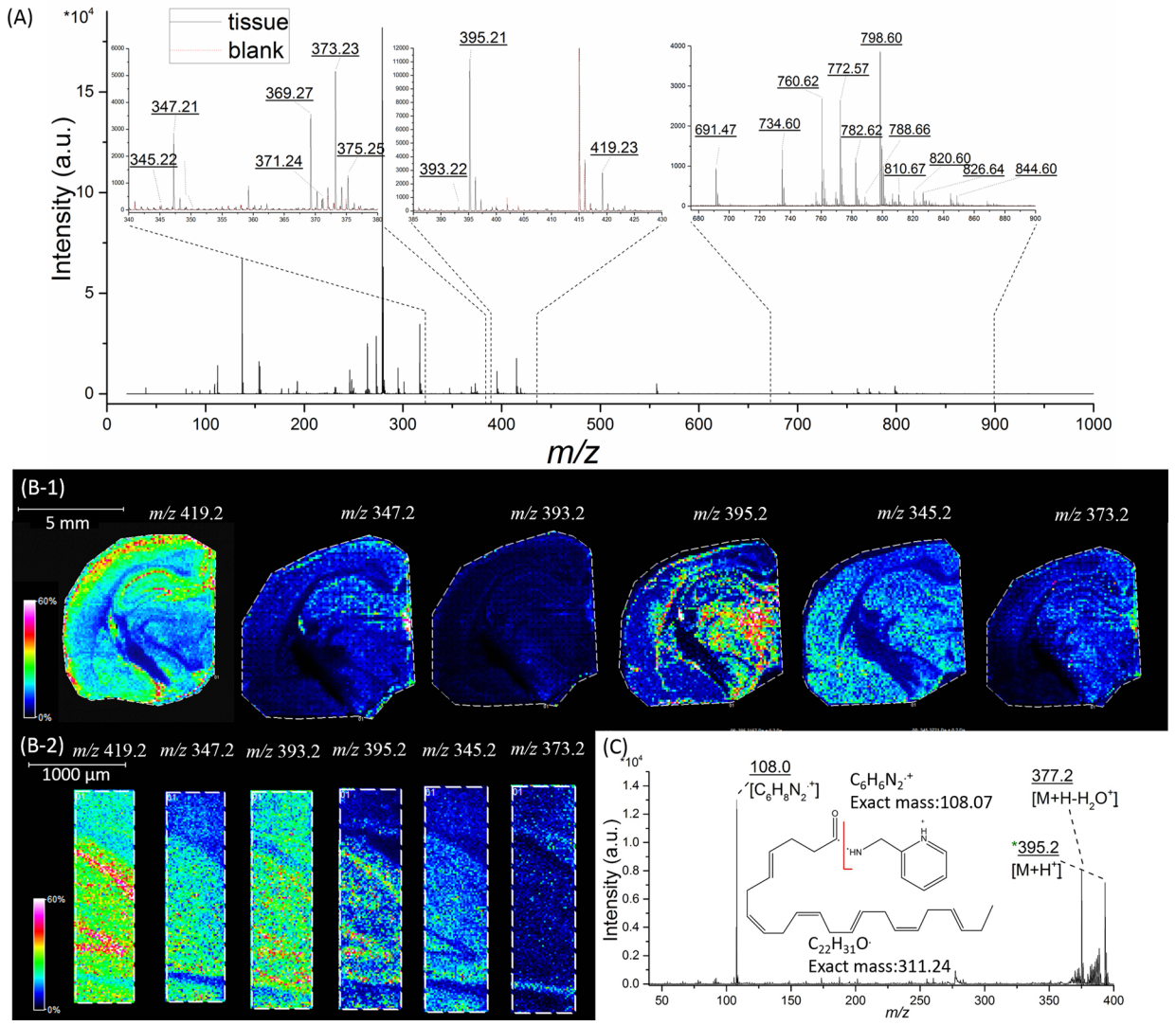

Figure 4. MSI ion maps and associated mass spectra obtained using the optimized electrospray on-tissue derivatization method. (A) Representative spectrum extracted from the rat cerebrum area. (B) MALDI MSI ion maps over an extended region at 100-μm spatial resolution (1), followed by 20-μm spatial resolution images (2) from selected subregions of the hippocampal area. (C) Representative MALDI MS/MS spectrum from the same tissue used to confirm the identity of AA.

many fatty acids can be difficult to determine given the possible occurrence of fatty acid isomers. In the case of DHA, we confirmed our assignment by examining its LC, MS, and MS/MS characteristics using a punch from an adjacent brain tissue slice. In this case, there are no obvious isomers of DHA in our samples (Figure S6). For the other fatty acids detected here, their structure was assigned via the MS and MS/MS data and by referring to prior reports that these specific fatty acids are found in the mouse brain using a variety of analytical methods.[22,30] Besides LC, ion mobility spectrometry can be coupled with MS, and fatty acid isomers may be isolated in real time during imaging.[55,56]

From the high-resolution MSI shown in Figure 4B-2, reconstructed ion images for DHA at m/z 419.2 and AA at m/z 395.2 show localization to the dentate gyrus granule cell layers and field CA1 pyramidal layer.[54] Eicosapentaenoic acid at m/z 393.2, palmitic acid at m/z 347.2, and palmitoleic acid at m/z 345.2 have complementary localizations with DHA and AA. While detectable with derivatization, no FFAs were detected in tissue without derivatization in positive mode. To demonstrate the reproducibility of this method with different animals, tissue slices from two more rats were examined using the same approach. Most of the FFAs were detected in cerebrum tissue of all three rats (Figure S7), and the relative levels and localization of those FFAs are similar.

Additionally, using electrospray as the deposition method, several high molecular weight lipids containing these FFAs were detectable both before (Figure 3D-3,E-3 and Figure S8A) and after (Figure 3D-2,E-2 and Figure S8C) on-tissue derivatization with similar spatial distributions and resolution. The ion images of two PCs at m/z 844.6 (Figure 3D) and m/z 872.6 (Figure 3E) (both possibly containing DHA[57]) are qualitatively unchanged following derivatization. MS/MS spectra of most of the detected PCs in Figure 4A are presented in Figure S9.

In order to quantify the changes in intensity and spatial distribution associated with derivatization, principal component analysis was performed for 12 lipids found in four anatomical regions (the MS and MS/MS spectra are shown in Figure 4A and Figure S9). As seen in Figure S10, spectra tended to group together in the score plot based on anatomical region, irrespective of derivatization. They also were well separated

DOI: 10.1021/acs.analchem.6b01021
Anal. Chem. 2016, 88, 5988−5995

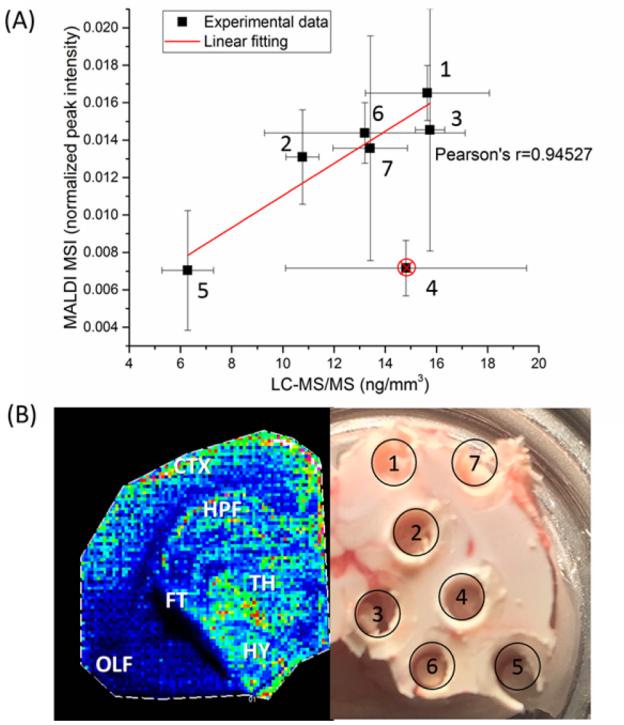

Figure 5. (A) Correlation between the average peak intensity of MALDI MSI (n = 3) versus the quantitation via LC−MS/MS results from different cerebrum regions (n = 3). (B) Locations used for the comparison: ion map of DHA abundance (using the same color scale as in Figure 4) and corresponding photo of brain tissue showing punched regions for the LC−MS/MS measurements. Labels 1 and 7, cortex, CTX; 2, hippocampal formation, HPF; 3, thalamus, TH; 4, fiber tract, FT; 5, olfactory area, OLF; 6, hypothalamus, HY.

from each other for some brain regions. To further characterize these lipids, tissues were also interrogated with MALDI MS/MS at the m/z values of potential lipid precursors (Figure S9). The main fragment at m/z 184 corresponds to the phosphocholine headgroup $[PO_3{-}CH_2{-}CH_2{-}N(CH_3)_3]^+$. Among the lipids, m/z 844.6 and 826.7 have additional fragments with a loss of m/z 59 corresponding to $[N(CH_3)_3]$. Previous studies on mouse brain utilized MS^3 to identify these masses as [PC(diacyl-16:0/22:6) + K]$^+$ and [PC(diacyl-18:0/18:1) + K]$^+$.[57] Many FFAs comprise the glycerophospholipids in cellular membranes, suggesting that the distributions of fatty acids should correlate with these lipids. Our derivatization method, by increasing the sensitivity of FFAs without changing lipid distributions, may help elucidate such spatial correlations.

Validation with LC−MS/MS. As MSI does not involve a separation technique, matrix effects and interference typically prevent quantitation of results. Furthermore, the derivatization yield may depend on the surrounding tissue properties. We thus used a complementary MS approach to compare ion abundance detected in various brain regions between MSI and a more conventional extraction, derivatization, and LC−MS/MS procedure. Tissues from the same brain cerebrum (Figure 5B) were prepared for MALDI MSI (Figure S11A) and for LC−MS/MS (Figure S11B). The punches were extracted with ethanol and derivatized in solution with the same derivatization chemistry and subsequently analyzed by LC−MS/MS. The MSI results (Figure S11A) were exported and the peak intensities in regions corresponding to the LC−MS/MS of the punches (Figure S11B) were grouped and averaged to generate an estimate of the intensity for each of the triplicate measurements. The MSI results were compared to the LC−MS/MS quantitative results (Figure 5A and Figure S11). As expected, the RSD of the on-tissue derivatization was high, at most 45%, but typically below 20%. From the comparison of mean values of the MSI and LC−MS/MS results for DHA, the data are correlated, with a correlation coefficient (r) of 0.945 (Figure 5A) (fiber tract regions were excluded due to a different composition/matrix effect compared to the other brain regions examined). A two sample t-test was performed between different regions for both the MSI and LC−MS/MS results. The distribution trends in different regions were similar between the two approaches, and some of the region pairs had significant differences ($p < 0.05$) for both the MSI and LC−MS/MS data from calculated FDR-corrected p values (e.g., the isocortex and olfactory areas). As LC−MS/MS provides quantitative data, the correlation between LC−MS/MS and MSI from distinct brain regions demonstrates the ability of our MALDI MSI approach to accurately provide semiquantitative fatty acid distributions when matrix effects are minimal.

CONCLUSIONS

MSI with on-tissue derivatization is an effective approach to improving the detectability of molecules with low ionization efficiency, such as fatty acids, via MALDI-TOF MS in positive mode. The use of electrospray-assisted derivatization and MALDI MSI provided the ability to detect nine FFAs, allowing us to distinguish these FFAs between distinct cell layers of the rat hippocampus, with an effective spatial resolution of about 20 μm. The MSI results were validated by quantitative LC−MS/MS, which displayed a correlation coefficient exceeding 0.9 between measurements from the two methods. We expect that electrospray-assisted derivatization will be effective with a number of different derivatization approaches, allowing enhanced detection and imaging of different classes of analytes.

ASSOCIATED CONTENT

Supporting Information

The Supporting Information is available free of charge on the ACS Publications website at DOI: 10.1021/acs.analchem.6b01021.

Additional experimental section, supporting Figures S1−S11, and Table S1 (PDF)

AUTHOR INFORMATION

Corresponding Author

*Phone: +1 217-244-7359. Fax: +1 217-265-6290. E-mail: jsweedle@illinois.edu.

Notes

The authors declare no competing financial interest.

ACKNOWLEDGMENTS

Funding was provided by Abbott Nutrition through the Center for Nutrition, Learning, and Memory, University of Illinois, Urbana−Champaign, and the National Institute on Drug Abuse by Award No. P30 DA018310. T.J.C. acknowledges funding from the Training Program at Chemistry-Interface with Biology (Grant T32 GM070421), the National Science Foundation Graduate Research Fellowship Program, and the Springborn Fellowship. The content is solely the responsibility of the authors and does not necessarily represent the official views of the funding agencies.

DOI: 10.1021/acs.analchem.6b01021
Anal. Chem. 2016, 88, 5988−5995

REFERENCES

(1) Caprioli, R. M.; Farmer, T. B.; Gile, J. *Anal. Chem.* **1997**, *69*, 4751−4760.
(2) Schwartz, S. A.; Caprioli, R. M. In *Mass Spectrometry Imaging: Principles and Protocols*, Rubakhin, S. S., Sweedler, J. V., Eds.; Humana: New York, 2010; pp 3−19.
(3) Liu, H. L.; Dai, J. Y.; Zhou, J. H.; Huang, H. Y.; Chen, F.; Liu, Z. L. *Int. J. Mass Spectrom.* **2015**, *376*, 85−89.
(4) Garrett, T. J.; Prieto-Conaway, M. C.; Kovtoun, V.; Bui, H.; Izgarian, N.; Stafford, G.; Yost, R. A. *Int. J. Mass Spectrom.* **2007**, *260*, 166−176.
(5) Chaurand, P.; Norris, J. L.; Cornett, D. S.; Mobley, J. A.; Caprioli, R. M. *J. Proteome Res.* **2006**, *5*, 2889−2900.
(6) Aksenov, A. A.; Bier, M. E. *J. Am. Soc. Mass Spectrom.* **2008**, *19*, 219−230.
(7) McDonnell, L. A.; Heeren, R. M. A. *Mass Spectrom. Rev.* **2007**, *26*, 606−643.
(8) Cornett, D. S.; Reyzer, M. L.; Chaurand, P.; Caprioli, R. M. *Nat. Methods* **2007**, *4*, 828−833.
(9) Zemski Berry, K. A.; Hankin, J. A.; Barkley, R. M.; Spraggins, J. M.; Caprioli, R. M.; Murphy, R. C. *Chem. Rev.* **2011**, *111*, 6491−6512.
(10) Goodwin, R. J. A.; Pennington, S. R.; Pitt, A. R. *Proteomics* **2008**, *8*, 3785−3800.
(11) Dekker, T. J. A.; Balluff, B. D.; Jones, E. A.; Schoene, C. D.; Schmitt, M.; Aubele, M.; Kroep, J. R.; Smit, V. T. H. B. M.; Tollenaar, R. A. E. M.; Mesker, W. E.; Walch, A.; McDonnell, L. A. *J. Proteome Res.* **2014**, *13*, 4730−4738.
(12) Rubakhin, S. S.; Jurchen, J. C.; Monroe, E. B.; Sweedler, J. V. *Drug Discovery Today* **2005**, *10*, 823−837.
(13) Hanrieder, J.; Phan, N. T. N.; Kurczy, M. E.; Ewing, A. G. *ACS Chem. Neurosci.* **2013**, *4*, 666−679.
(14) Kinumi, T.; Saisu, T.; Takayama, M.; Niwa, H. *J. Mass Spectrom.* **2000**, *35*, 417−422.
(15) Goodwin, R. J. A. *J. Proteomics* **2012**, *75*, 4893−4911.
(16) Itoh, Y.; Kawamata, Y.; Harada, M.; Kobayashi, M.; Fujii, R.; Fukusumi, S.; Ogi, K.; Hosoya, M.; Tanaka, Y.; Uejima, H.; Tanaka, H.; Maruyama, M.; Satoh, R.; Okubo, S.; Kizawa, H.; Komatsu, H.; Matsumura, F.; Noguchi, Y.; Shinohara, T.; Hinuma, S.; et al. *Nature* **2003**, *422*, 173−176.
(17) Hua, Y.; Dagan, S.; Wickramasekara, S.; Boday, D. J.; Wysocki, V. H. *J. Mass Spectrom.* **2010**, *45*, 1394−1401.
(18) Park, K.-H.; Kim, H.-J. *Rapid Commun. Mass Spectrom.* **2001**, *15*, 1494−1499.
(19) Langley, G. J.; Herniman, J. M.; Townell, M. S. *Rapid Commun. Mass Spectrom.* **2007**, *21*, 180−190.
(20) Borissova, M.; Palk, K.; Vaher, M. *Procedia Chem.* **2010**, *2*, 174−179.
(21) Sekula, J.; Niziol, J.; Misiorek, M.; Dec, P.; Wrona, A.; Arendowski, A.; Ruman, T. *Anal. Chim. Acta* **2015**, *895*, 45−53.
(22) Dufresne, M.; Thomas, A.; Breault-Turcot, J.; Masson, J.-F.; Chaurand, P. *Anal. Chem.* **2013**, *85*, 3318−3324.
(23) Liu, Y.; Liu, J.; Deng, C.; Zhang, X. *Rapid Commun. Mass Spectrom.* **2011**, *25*, 3223−3234.
(24) Crecelius, A.; Clench, M. R.; Richards, D. S.; Parr, V. *J. Chromatogr.* **2002**, *958*, 249−260.
(25) Lauzon, N.; Dufresne, M.; Chauhan, V.; Chaurand, P. *J. Am. Soc. Mass Spectrom.* **2015**, *26*, 878−886.
(26) Morosi, L.; Spinelli, P.; Zucchetti, M.; Pretto, F.; Carra, A.; D'Incalci, M.; Giavazzi, R.; Davoli, E. *PLoS One* **2013**, *8*, e72532.
(27) Kurczy, M. E.; Zhu, Z.-J.; Ivanisevic, J.; Schuyler, A. M.; Lalwani, K.; Santidrian, A. F.; David, J. M.; Giddabasappa, A.; Roberts, A. J.; Olivos, H. J.; O'Brien, P. J.; Franco, L.; Fields, M. W.; Paris, L. P.; Friedlander, M.; Johnson, C. H.; Epstein, A. A.; Gendelman, H. E.; Wood, M. R.; Felding, B. H. *Nat. Commun.* **2015**, *6*, 5998.
(28) Amaya, K. R.; Sweedler, J. V.; Clayton, D. F. *J. Neurochem.* **2011**, *118*, 499−511.
(29) Richter, K.; Nygren, H.; Malmberg, P.; Hagenhoff, B. *Microsc. Res. Tech.* **2007**, *70*, 640−647.
(30) Guo, S.; Wang, Y.; Zhou, D.; Li, Z. *Anal. Chem.* **2015**, *87*, 5860−5865.
(31) Schwartz, S. A.; Reyzer, M. L.; Caprioli, R. M. *J. Mass Spectrom.* **2003**, *38*, 699−708.
(32) Toue, S.; Sugiura, Y.; Kubo, A.; Ohmura, M.; Karakawa, S.; Mizukoshi, T.; Yoneda, J.; Miyano, H.; Noguchi, Y.; Kobayashi, T.; Kabe, Y.; Suematsu, M. *Proteomics* **2014**, *14*, 810−819.
(33) Manier, M. L.; Reyzer, M. L.; Goh, A.; Dartois, V.; Via, L. E.; Barry, C. E., 3rd; Caprioli, R. M. *J. Am. Soc. Mass Spectrom.* **2011**, *22*, 1409−1419.
(34) Franck, J.; El Ayed, M.; Wisztorski, M.; Salzet, M.; Fournier, I. *Anal. Chem.* **2009**, *81*, 8305−8317.
(35) Shariatgorji, M.; Nilsson, A.; Goodwin, R. J. A.; Kallback, P.; Schintu, N.; Zhang, X.; Crossman, A. R.; Bezard, E.; Svenningsson, P.; Andren, P. E. *Neuron* **2014**, *84*, 697−707.
(36) Shariatgorji, M.; Nilsson, A.; Kallback, P.; Karlsson, O.; Zhang, X.; Svenningsson, P.; Andren, P. E. *J. Am. Soc. Mass Spectrom.* **2015**, *26*, 934−939.
(37) Cobice, D. F.; Mackay, C. L.; Goodwin, R. J.; McBride, A.; Langridge-Smith, P. R.; Webster, S. P.; Walker, B. R.; Andrew, R. *Anal. Chem.* **2013**, *85*, 11576−11584.
(38) Manier, M. L.; Spraggins, J. M.; Reyzer, M. L.; Norris, J. L.; Caprioli, R. M. *J. Mass Spectrom.* **2014**, *49*, 665−673.
(39) McNeal, C. J.; Macfarlane, R. D.; Thurston, E. L. *Anal. Chem.* **1979**, *51*, 2036−2039.
(40) Fenn, J. B.; Mann, M.; Meng, C. K.; Wong, S. F.; Whitehouse, C. M. *Mass Spectrom. Rev.* **1990**, *9*, 37−70.
(41) Kebarle, P.; Tang, L. *Anal. Chem.* **1993**, *65*, 972A−986A.
(42) Jurchen, J. C.; Rubakhin, S. S.; Sweedler, J. V. *J. Am. Soc. Mass Spectrom.* **2005**, *16*, 1654−1659.
(43) Kruse, R.; Sweedler, J. V. *J. Am. Soc. Mass Spectrom.* **2003**, *14*, 752−759.
(44) Higashi, T.; Ichikawa, T.; Inagaki, S.; Min, J. Z.; Fukushima, T.; Toyo'oka, T. *J. Pharm. Biomed. Anal.* **2010**, *52*, 809−818.
(45) Toyo'oka, T.; Ishibashi, M.; Takeda, Y.; Nakashima, K.; Akiyama, S.; Uzu, S.; Imai, K. *J. Chromatogr.* **1991**, *588*, 61−71.
(46) Hankin, J. A.; Barkley, R. M.; Murphy, R. C. *J. Am. Soc. Mass Spectrom.* **2007**, *18*, 1646−1652.
(47) Lanni, E. J.; Dunham, S. J. B.; Nemes, P.; Rubakhin, S. S.; Sweedler, J. V. *J. Am. Soc. Mass Spectrom.* **2014**, *25*, 1897−1907.
(48) Mayer, P.; Vaes, W. H. J.; Hermens, J. L. M. *Anal. Chem.* **2000**, *72*, 459−464.
(49) Ai, J. *Anal. Chem.* **1997**, *69*, 1230−1236.
(50) Chen, X. P.; Cheng, J. S.; Yin, X. Z. In *Optical Technology and Image Processing for Fluids and Solids Diagnostics 2002*; Shen, G. X., Cha, S. S., Chiang, F. P., Mercer, C. R., Eds.; SPIE-Int. Soc. Opt. Eng.: Bellingham, WA, 2002; pp 181−187.
(51) Wilhelm, O.; Mädler, L.; Pratsinis, S. E. *J. Aerosol Sci.* **2003**, *34*, 815−836.
(52) Venter, A.; Sojka, P. E.; Cooks, R. G. *Anal. Chem.* **2006**, *78*, 8549−8555.
(53) Rietveld, I. B.; Kobayashi, K.; Yamada, H.; Matsushige, K. *J. Phys. Chem. B* **2006**, *110*, 23351−23364.
(54) Lein, E. S.; Hawrylycz, M. J.; Ao, N.; Ayres, M.; Bensinger, A.; Bernard, A.; Boe, A. F.; Boguski, M. S.; Brockway, K. S.; Byrnes, E. J.; Chen, L.; Chen, L.; Chen, T.-M.; Chi Chin, M.; Chong, J.; Crook, B. E.; Czaplinska, A.; Dang, C. N.; Datta, S.; Dee, N. R.; et al. *Nature* **2007**, *445*, 168−176.
(55) Zhang, F.; Guo, S.; Zhang, M.; Zhang, Z.; Guo, Y. *J. Mass Spectrom.* **2015**, *50*, 906−913.
(56) Leng, J.; Guan, Q.; Sun, T.; Wang, H.; Cui, J.; Liu, Q.; Zhang, Z.; Zhang, M.; Guo, Y. *Anal. Chim. Acta* **2015**, *887*, 148−154.
(57) Sugiura, Y.; Konishi, Y.; Zaima, N.; Kajihara, S.; Nakanishi, H.; Taguchi, R.; Setou, M. *J. Lipid Res.* **2009**, *50*, 1776−1788.

DOI: 10.1021/acs.analchem.6b01021
Anal. Chem. 2016, 88, 5988−5995